AIAA JOURNAL
Vol. 43, No. 11, November 2005

Acoustic Resonances in Rectangular Open Cavities

W. Koch*
DLR, German Aerospace Center, D37073 Göttingen, Germany

Acoustic resonances are computed numerically in rectangular two-dimensional deep and shallow open cavities. Unconfined cavities as well as cavities confined in a two-dimensional infinitely long duct are considered. Because of radiation losses these resonances are generally complex valued. All computations are made for zero mean flow. Perfectly matched layer absorbing boundary conditions are employed to avoid unphysical reflections at the necessarily finite grid boundaries. In confined cavities a few resonant modes, so-called trapped modes, exist with zero radiation losses, and significant differences are observed between confined and unconfined cavity resonances. A comparison with the frequencies of the modes observed by Rossiter suggests that the dominant Rossiter modes lock in at resonant cavity frequencies.

Nomenclature

c_0^*	=	ambient speed of sound
d	=	depth of cavity, d^*/l_{ref}^*
d_x, d_y	=	perfectly matched layer (PML) width in (x, y) direction
f^*	=	frequency
h	=	height of channel, h^*/l_{ref}^*
i	=	imaginary unit
K	=	dimensionless frequency, $\omega^* l^*/c_0^*$
K_1	=	dimensionless frequency, $\omega^* h^*/c_0^*$
l	=	length of cavity, l^*/l_{ref}^*
l_{ref}^*	=	reference length, l^* or h^*
M	=	Mach number
m, n	=	cavity mode numbers
$N_{x,\text{col}}$, $N_{y,\text{col}}$	=	number of Chebyshev collocation points in (x, y) direction
p	=	acoustic pressure, $p^*/\rho_0^* c_0^{*2}$
t^*	=	time
u, v	=	acoustic velocity components in (x, y) direction, u^*/c_0^*, v^*/c_0^*
x, y	=	Cartesian coordinates, x^*/l_{ref}^*, y^*/l_{ref}^*
$\pm x_0$, $\pm y_0$	=	beginning of PML in (x, y) direction
β	=	PML shape parameter, 1
γ	=	ratio of specific heats, c_p/c_v
ξ, η	=	scaled complex coordinates in PML
ρ_0^*	=	ambient density
$\sigma_x(x)$, $\sigma_y(y)$	=	PML damping functions in (x, y) direction
$\sigma_{0,x}$, $\sigma_{0,y}$	=	PML damping constants in (x, y) direction
$\phi(x, y)$	=	acoustic velocity potential
ω^*	=	circular frequency, $2\pi f^*$

Superscript

$*$	=	dimensional quantity

I. Introduction

SELF-EXCITED flow oscillations occur in many industrial, aeronautical, or marine applications. The ensuing highly unsteady loadings may lead to considerable drag increase, structural vibrations, or unacceptably high noise levels. The sources of these self-excited oscillations are usually globally unstable wakes or convectively unstable jets and shear layers that become globally unstable through an upstream feedback mechanism after impinging on a downstream obstacle.[1–4] If the acoustic wavelength is in the same order or smaller than the characteristic length of the device, the aforementioned flow oscillations can be enhanced or even dominated by acoustic standing-wave resonances. In this case the frequency of the flow oscillation can lock in at the resonant frequency and high pressure amplitudes may be observed. Standing-wave resonances without flow are also of importance in diffraction and scattering problems. In hydrology, standing surface waves in an enclosed (lake) or semi-enclosed (harbor or bay) body of water are termed seiches.

The objective of the present paper is to numerically compute acoustic resonances in rectangular two-dimensional open cavities. We neglect mean flow effects because we expect that our no-flow results approximate the resonant frequencies at low Mach numbers. The original investigations of unsteady flow past cavities were motivated by buffeting problems in bomb bays.[5,6] Rossiter[6] pointed out that the periodic pressure fluctuations in the flow past a cavity are caused by a feedback phenomenon similar to that which produces edge tones. He proposed a still widely used semi-empirical prediction formula for the Strouhal number of these multistage feedback modes, which are now known as Rossiter modes. After several improvements (see, e.g., Bilanin and Covert,[7] Heller and Bliss,[8] Tam and Block,[9] or Howe,[10] to mention just a few), this linear feedback model reached a certain maturity with the global analysis of Alvarez et al.[11] Extensive experimental cavity noise results were documented by Ahuja and Mendoza[12] to serve as benchmark data for the validation of computational aeroacoustics codes.

By combining propagation models in the central region of the cavity with scattering models for the end regions, Alvarez et al.[11] were able to formulate a global eigenvalue problem that allows coupling of the Rossiter modes with acoustic resonances without any empirical constants. In a forthcoming paper[13] this method is applied to the case of a cavity in a wind tunnel with results confirming our present findings (see also Ref. 14) that a duct environment can significantly alter cavity tones. The exact scattering processes in Ref. 11 are determined via the analytical Wiener–Hopf technique, which is limited to special geometries. Contrary to this our numerical method can be applied to arbitrary configurations, which will be demonstrated in our forthcoming paper.[15]

A central hypothesis of the present paper is that the Rossiter modes provide the sound source mechanism and can be enhanced by standing-wave acoustic resonances. Although Alvarez et al.[11] are able to compute the positive or negative gain at the Rossiter frequencies, we can only calculate the acoustic cavity resonances and determine the one with the lowest radiation loss (i.e., the one that might dominate if excited by the Rossiter mechanism). A definite drawback of our analysis is the neglect of mean flow. However, it has been shown by Hu[16] that mean flow can be included in a PML

Presented as Paper 2004-2843 at the AIAA/CEAS 10th Aeroacoustics Conference, Manchester, England, United Kingdom, 10–12 May 2004; received 10 November 2004; revision received 10 May 2005; accepted for publication 11 May 2005.

*Research Scientist, Institute for Aerodynamics and Flow Technology, Bunsenstrasse 10. Member AIAA.

computation. This will be done in future investigations. The main problem is how to obtain the correct mean flow (especially if the flow is turbulent), a problem which is also of concern in the analysis of Alvarez et al.[11] One can either model the mean flow or take it from experiment or numerical computation. As can be seen from Ref. 11, this can be quite successful. A remaining problem is the computation of the nonlinear saturation amplitude. This is beyond these linear analyses and requires a nonlinear numerical treatment.[17,18] If the distance between the upstream and downstream edge of the cavity is large, the upstream edge of the cavity acts like a backward-facing step and the flow oscillations change to the so-called wake mode with large-scale vortex shedding and considerable increase in drag.[18,19]

Krishnamurty[20] already observed in his experiments that the flow over cavities can lead to strong acoustic radiation, and it is well known that cavity noise constitutes an annoying part of airframe noise.[21] The early papers on cavity noise mentioned the occurence of standing waves, but standing-wave resonances became of interest again only recently in connection with increased efforts in actively controlling cavity oscillations.[22,23] From a resonance point of view, and neglecting three-dimensional width effects, one distinguishes between deep ($l^*/d^* < 1$) and shallow ($l^*/d^* > 1$) cavities,[1,24] where l^* denotes the streamwise length and d^* the depth of the cavity. Here and in the following, the superscript asterisk indicates dimensional quantities whereas quantities without an asterisk are nondimensional. In deep cavities it is mainly transverse depth modes that are excited, whereas in shallow cavities the longitudinal modes prevail.

Plumblee et al.[5] provided a first approximation for the resonant response of deep cavities, and the low-Mach-number results of deep cavities were found to center around this depthwise cavity resonance.[9,22,25,26] At the predominant mode (i.e., dominant in terms of amplitude), Rossiter[6] also observed standing-wave patterns for shallow cavities. Furthermore, he found that the corresponding frequencies cluster in frequency bands. But it was Rockwell and Naudascher[1] who demonstrated that these bands are close to the longitudinal cavity resonances (cf. the experiments of Shaw et al.[27] for large enclosures with a small opening). For the no-flow situation these natural frequencies are identical to the semi-analytical result of Tam,[28] who computed several two-dimensional resonances of rectangular open cavities for $l^*/d^* \leq 1$. Recently, natural acoustic modes also were found to correlate jet–cavity interaction tones.[29]

The normal modes of unconfined shallow cavities are highly damped by radiation losses such that high-energy sources are necessary to excite them. Shear layers can provide this energy only at higher Mach numbers. However, if the cavity is confined in a channel, the radiation losses of shallow cavities can be reduced considerably, making these modes more susceptible to shear-layer excitation even at low Mach numbers.[30] Evans and Linton[31] were the first to demonstrate that a few modes exist even with zero radiation losses. These so-called trapped modes are resonant modes that decay toward infinity and therefore do not radiate.

A basic difficulty in numerically computing resonances in open domains is the radiation of energy to infinity. The infinite domain has to be truncated and this causes unphysical wave reflections at the boundaries of the computational grid. As a consequence the results are useless unless nonreflecting or absorbing boundary conditions are employed. Here the PML technique of Bérenger[32] became the preferred method for electromagnetic and acoustic wave propagation problems. A disadvantage of the PML method is that the computational domain is enlarged considerably by the unphysical PML region and thus requires larger solution vectors. The older complex scaling method of atomic and molecular physics (cf. the recent review by Moiseyev[33]) is very similar to the PML method and will be employed in our investigation. Both the PML and the complex scaling method reduce the computation of resonances to the computation of eigenvalues.

II. Governing Equation and Solution Procedure

The equation governing small disturbances in a medium with zero mean flow is the wave equation. In the following all lengths will be nondimensionalized with a characteristic reference length l^*_{ref}, velocities with the ambient speed of sound c^*_0, densities with the ambient density ρ^*_0, and pressures with $\rho^*_0 c^{*2}_0$. Assuming periodic time dependence $\exp(-i\omega^* t^*)$, where ω^* is the circular frequency, the wave equation can be reduced to the Helmholtz equation for the velocity potential $\phi(x, y)$:

$$\left(\frac{\partial^2}{\partial x^2} + \frac{\partial^2}{\partial y^2}\right)\phi(x, y) + K^2\phi(x, y) = 0 \tag{1}$$

where x, y are the nondimensional Cartesian coordinates in two dimensions and $K = \omega^* l^*_{\text{ref}}/c^*_0$ denotes the dimensionless frequency, with $K/2\pi$ being the Helmholtz number.[34] The time-independent dimensionless disturbance velocity and pressure are then given by $\boldsymbol{v}(x, y) = \nabla\phi$ and $p(x, y) = iK\phi$, respectively.

In addition to the hard-wall boundary conditions the radiation condition has to be satisfied. Numerically this can be implemented by the complex scaling method,[33] an earlier version of the PML method. For two-dimensional Cartesian coordinates the complex scaling method works as follows: in the PML domain, $\phi(x, y)$ is continued analytically with respect to the variables $(x, y) \in \mathbb{R}^2$ to the complex variables $(\xi, \eta) \in \mathbb{C}^2$. The extended solution $\tilde{\phi}(\xi, \eta)$ satisfies the same differential equation as $\phi(x, y)$; that is,

$$\left(\frac{\partial^2}{\partial \xi^2} + \frac{\partial^2}{\partial \eta^2}\right)\tilde{\phi}(\xi, \eta) + K^2\tilde{\phi}(\xi, \eta) = 0 \tag{2}$$

For ξ and η we consider the paths

$$\xi(x) = x + i\sigma_x(x), \qquad \eta(y) = y + i\sigma_y(y) \tag{3}$$

The spatial variation of damping functions $\sigma_x(x)$ and $\sigma_y(y)$ is usually chosen in power form, smoothly starting at the PML interface, say at $x = \pm x_0$ in the x direction, or $y = \pm y_0$ in the y direction; for example,

$$\sigma_x(x) = \begin{cases} \sigma_{0,x}(x - x_0)^\beta, & x > x_0 \\ 0, & |x| \leq x_0 \\ -\sigma_{0,x}(-x - x_0)^\beta, & x < -x_0 \end{cases} \tag{4}$$

$$\sigma_y(y) = \begin{cases} \sigma_{0,y}(y - y_0)^\beta, & y > y_0 \\ 0, & |y| \leq y_0 \\ -\sigma_{0,y}(-y - y_0)^\beta, & y < -y_0 \end{cases} \tag{5}$$

with damping coefficients $\sigma_{0,x} > 0$, $\sigma_{0,y} > 0$ and a shape parameter $\beta \geq 1$. In Ref. 35 we found $\beta = 1$ to be the best choice.

Using the chain rule, the function $\phi_{\text{PML}}(x, y) := \tilde{\phi}(\xi(x), \eta(y))$ satisfies the elliptic differential equation

$$\frac{1}{\xi'(x)}\frac{\partial}{\partial x}\left[\frac{1}{\xi'(x)}\frac{\partial \phi_{\text{PML}}}{\partial x}\right] + \frac{1}{\eta'(y)}\frac{\partial}{\partial y}\left[\frac{1}{\eta'(y)}\frac{\partial \phi_{\text{PML}}}{\partial y}\right] + K^2\phi_{\text{PML}} = 0 \tag{6}$$

It can be seen that ϕ is outgoing if and only if $\phi_{\text{PML}}(x, y)$ decays exponentially as $|x| \to \infty$ and $|y| \to \infty$. This suggests imposing homogeneous Dirichlet conditions at some finite distances $\pm(x_0 + d_x)$ and $\pm(y_0 + d_y)$:

$$\phi_{\text{PML}}(\pm(x_0 + d_x), y) = 0, \qquad \phi_{\text{PML}}(x, \pm(y_0 + d_y)) = 0 \tag{7}$$

where d_x and d_y are the widths of the PML in the x and y directions, respectively. With PMLs, the problem just defined constitutes a homogeneous boundary-value problem in a finite domain. For the corresponding numerical solution we discretize the problem by means of a two-dimensional multidomain Chebyshev collocation method[36] with $N_{x,\text{col}}$ and $N_{y,\text{col}}$ collocation points in x and y directions in each domain. The resulting algebraic eigenvalue problem is then solved directly or iteratively using standard algorithms.

III. Unconfined Cavity

Cavities can be confined in a duct or can be open to free space. First we consider a two-dimensional unconfined rectangular cavity in a semi-infinite wall as sketched in Fig. 1a. As reference length l^*_{ref} we choose the cavity length l^*. Then $l = 1$ is the (nondimensional) cavity length and d denotes the (nondimensional) depth of the cavity. Without flow there is symmetry about the y axis, and we only have to solve for $x \geq 0$ by applying symmetry and antisymmetry conditions at $x = 0$. At the same time this can be thought of as a gap of width l in a screen of thickness $2d$ as indicated by the dashed lines in Fig. 1a. In the gap case only the quarter-plane problem needs to be solved by imposing both symmetry and antisymmetry conditions at the bottom of the cavity (i.e., $y = -d$). For the cavity problem only the symmetry condition is relevant. The PMLs in the x and y directions start at x_0 and y_0, respectively, have thicknesses d_x and d_y, and are characterized by damping functions σ_x and σ_y as depicted in Fig. 1.

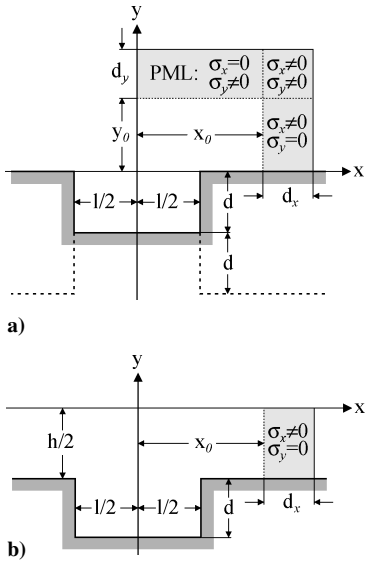

Fig. 1 Rectangular cavity with PMLs: a) unconfined and b) confined.

Figure 2a shows the spectrum of the symmetric $[\phi(-x, y) = \phi(+x, y)]$ and antisymmetric $[\phi(-x, y) = -\phi(+x, y)]$ cavity resonances for the deep cavity case ($l/d = 0.5$). All spectra in Fig. 2 were computed with $N_{x,\text{col}} = N_{y,\text{col}} = 30$, $d_x = d_y = 1.0$, $\sigma_{0,x} = \sigma_{0,y} = 5.0$, $\beta = 1$, $x_0 = 1.5$, and $y_0 = 1.0$; circles denote symmetric modes and triangles denote antisymmetric modes. The real part of the nondimensional frequency, $\text{Re}(K/2\pi)$, corresponds to the resonant frequency and the imaginary part, $\text{Im}(K/2\pi)$, is a measure for the radiation loss. The symbols very close to the imaginary axis are the discrete approximation of the continuous spectrum. Each resonant mode can be denoted by (m, n), where $m = 0, 1, \ldots,$ is the number of cavity pressure nodes in the x direction (longitudinal mode number) and $n = 0, 1, \ldots,$ is the number of cavity pressure nodes in the y direction (depth mode number). Tam[28] considered only the modes $(0, n)$ and $(1, n)$ ($n = 0, 1, 2, 3$; note that Tam used a different mode numbering: $m' = m + 1$, $n' = n + 1$). The crosses in Fig. 2 mark Tam's semi-analytic values listed in his Tables 1–4. The slight discrepancies for the higher damped modes are probably due to our chosen PML parameters. The physically more important weakly damped modes are practically identical. We see that the higher longitudinal cavity modes have much lower radiation losses than the higher deep-cavity modes; however, they occur at higher frequencies. Also shown in Fig. 2a are sample eigenfunctions (real

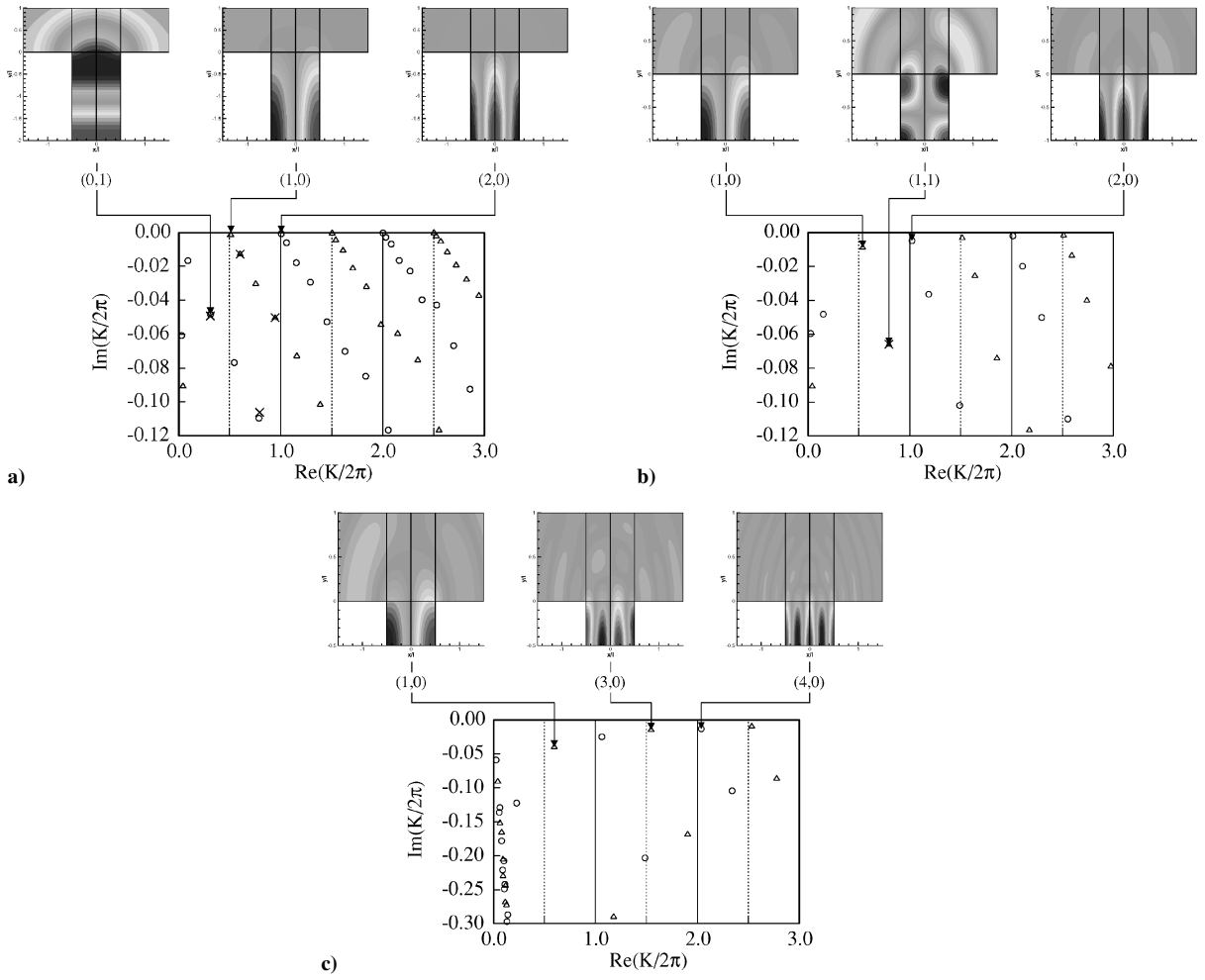

Fig. 2 Unconfined cavity resonances with sample eigenfunctions (scales of the horizontal and vertical axes of the Tecplot eigenfunction plots are independent of each other): a) deep cavity, $l/d = 0.5$; b) square cavity, $l/d = 1.0$; and c) shallow cavity, $l/d = 2.0$.

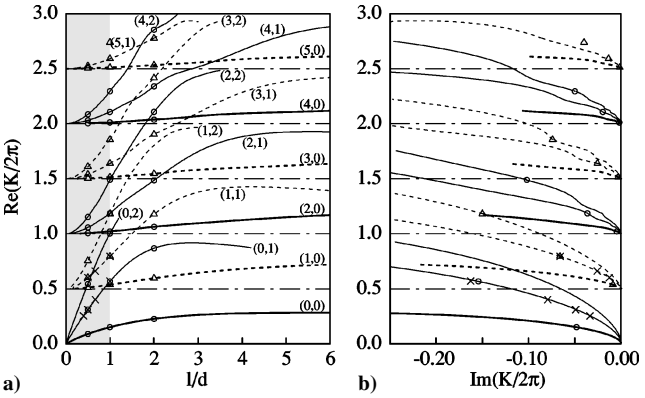

Fig. 3 Resonant frequencies of unconfined cavity modes (m, n): a) variation of resonant frequency with l/d and b) damping $\mathrm{Im}(K/2\pi)$ of the resonant modes.

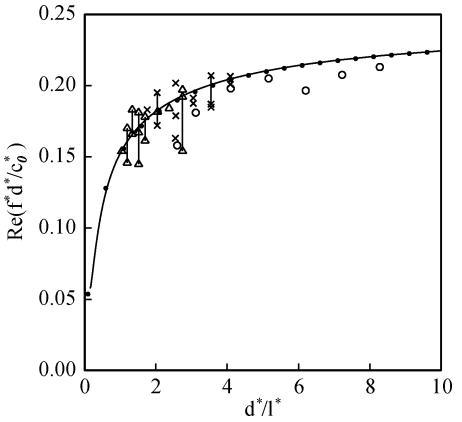

Fig. 4 Comparison of East's[25] experimental results (open symbols) with our fundamental (0, 0) resonant frequency (solid curve). The solid dots show the results of East's empirical formula [Eq. (8)].

part of ϕ), namely the second depth mode (0, 1), and the first antisymmetric and first symmetric longitudinal mode (1, 0) and (2, 0), respectively. The spectral pattern of Fig. 2a is strikingly similar to that of laser modes between two mirrors,[35] where the high-frequency longitudinal modes also have the lowest radiation losses.

Figure 2b depicts the spectrum of the square-cavity resonances with $l/d = 1$, which traditionally marks the bounding case between deep and shallow cavities. Again the radiation losses decrease with increasing longitudinal mode number, but they are much higher than for $l/d = 0.5$. Instead of the sample eigenfunction (0, 1) of Fig. 2a, we now picture (1, 1). Finally, Fig. 2c shows the spectrum of the cavity resonances for the shallow cavity, $l/d = 2$, together with higher order longitudinal eigenfunctions. The radiation losses are much higher. (Notice the different scale of the imaginary axis.) The discrete approximation of the continuous spectrum near the imaginary axis is now more clearly visible.

Each resonant eigenvalue in the preceding figures can now be continued iteratively to other l/d ratios, for example via Wielandt iteration (see Ref. 37, pp. 289ff). Using the lower resolution $N_{x,\mathrm{col}} = N_{y,\mathrm{col}} = 20$, the resulting resonant frequencies $\mathrm{Re}(K/2\pi)$ of the first few modes (m, n) are depicted in Fig. 3a up to $l/d = 6$, with the corresponding damping shown in Fig. 3b. This way the quality factor $Q = |\mathrm{Re}(K)/[2\mathrm{Im}(K)]|$ can be computed for each mode. The wavy curves in Fig. 3b for the higher modes look suspiciously like an underresolved solution. However, using $N_{x,\mathrm{col}} = N_{y,\mathrm{col}} = 30$ and $d_x = d_y = 4.0$ gave practically identical results. Unfortunately Tam[28] did not compute these higher longitudinal modes, but his deep-cavity resonances for modes (0, 1) and (1, 1) are marked by the crosses. The shaded area outlines the range of deep-cavity parameters. The solid lines depict the resonances of symmetric eigenfunctions, the dashed lines the resonances of antisymmetric eigenfunctions.

The open symbols in Fig. 3a repeat the resonant frequencies of Fig. 2. In Fig. 3b only the symbols for $l/d = 1$ are included. The higher depth modes become rapidly damped as l/d increases and the accuracy of these higher depth modes diminishes with increasing l/d. Therefore, these modes are discontinued when their accuracy becomes dubious, which is the case for large damping (cf. Fig. 2a). Physically they should be of less importance anyway due to their high radiation losses. On the other hand, the higher longitudinal modes $(1, 0), \ldots, (5, 0)$ (marked by thick lines) are only weakly damped (cf. Fig. 3b or Fig. 2). In Fig. 3a we see that for $l/d < 1$ several depth mode resonances $(0, n)$ occur with increasing frequency before the first longitudinal mode (1, 0) resonance is reached. At $l/d \approx 1$ this reverses: then the first (antisymmetric) longitudinal mode (1, 0) occurs for lower frequencies than the first depth mode (0, 1) resonance. This is the reason why the square cavity $d/l = 1$ is customarily considered to divide deep cavities from shallow cavities.[1]

The no-flow results of Fig. 3 can be used to check whether these standing-wave resonances are close to any of the observed dominating discrete frequencies excited by the flow over a cavity. In doing so we assume that the influence of the flow on the resonances is small, which is plausible for low-Mach-number flows. For such flows the works by Plumblee et al.,[5] East,[25] and Tam and Block[9,26] have already demonstrated that the discrete frequencies of deep-cavity noise cluster around the fundamental resonance. This is reconfirmed by Fig. 4, which shows East's[25] experimental deep-cavity results together with our theoretical curve for the fundamental resonance (0, 0). Our result is identical with the semi-analytical result of Tam[28] and is practically indistinguishable from the approximations of Plumblee et al.[5] as well as the data obtained via East's[25] empirical formula

$$\frac{f^* d^*}{c_0^*} = \frac{0.25}{1 + 0.65(l^*/d^*)^{0.75}} \tag{8}$$

For cavities with $l/d = 1$ and 2, Rossiter[6] observed standing-wave patterns. He called these modes I, II, and III and stated that they do not correspond to the feedback modes. He found that all predominant frequencies of cavity noise (i.e., dominant in terms of amplitude) clustered in the (approximately constant) frequency bands of these modes. Rockwell and Naudascher[1] related these frequency bands to the longitudinal resonances of the shallow cavity, but they assumed a closed cavity to compute the resonances. Our solution also gives the radiation damping. In Fig. 5 our open-cavity resonances of Fig. 3a are compared with the experimental data of Rossiter.[6] The data points of Rossiter's predominant frequencies are marked by filled circles. To convert Rossiter's dimensional data into nondimensional form we assumed an ambient speed of sound of $c_0^* = 340$ m/s.

Also included are the first few Rossiter modes according to Rossiter's[6] semi-empirical formula

$$\frac{K}{2\pi} = M \frac{c}{c_0} \frac{j - \gamma_R}{1/K_R + M} \tag{9}$$

where M denotes the freestream Mach number and c the corresponding speed of sound. The integer mode number j indicates the number of vortices spanning the cavity length. Rossiter's semi-empirical constants γ_R and K_R represent the phase shift of the acoustic scattering process at the downstream edge and the ratio of the convective speed of the vortices to the freestream velocity, respectively. Rossiter[6] used the empirically found values $\gamma_R = 0.25$, $K_R = 0.66$ for $l/d = 2$, and $K_R = 0.61$ for $l/d = 1$. In the analysis of Alvarez et al.[11] no empiricism is needed. The speed of sound c changes with M according to

$$c/c_0 = \{1 + [(\gamma - 1)/2]M^2\}^{-\frac{1}{2}} \tag{10}$$

where $\gamma = c_p/c_v$ is the ratio of the specific heats. Even though our resonances were computed for zero mean flow they are fairly close to the frequencies of Rossiter's predominant modes up to $M = 1.2$, as postulated already by Rockwell and Naudascher.[1] One reason for the good agreement might be that the resonant eigenfunctions

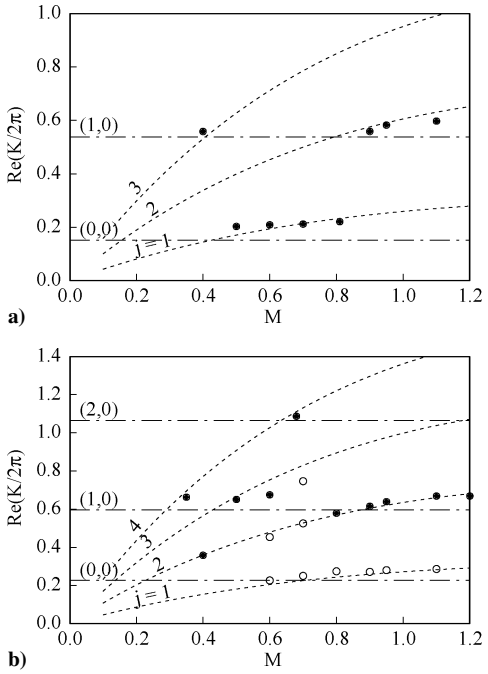

Fig. 5 Comparison of Rossiter's[6] experimental data (symbols) with the Rossiter modes (dashed curves) and our no-flow resonances (m, 0): a) $l/d = 1$ and b) $l/d = 2$.

are more or less confined to the cavity (cf. Fig. 2), where the mean flow is practically zero. However, this is still surprising and might be fortuitous, because other important effects like three-dimensionality or axial and lateral confinement are not included in our computation. In the following section we study the effect of lateral confinement.

IV. Confined Cavity

In this section we consider resonances in two-dimensional cavities that are confined in an infinitely long duct as sketched in Fig. 1b. By confinement we mean that there exists an acoustically reflecting wall and the cavity can no longer radiate freely in all directions, only along the duct axis. Cavity radiation losses can be reduced considerably and aerodynamic excitation of shallow cavities is also possible at low Mach numbers. For deep cavities such configurations are known to lead to strong flow-excited resonances in pipe systems with closed sidebranches[38–40] or regulating valves.[41,42] The relevant reference length l^*_{ref} is now the channel height h^* (i.e., $h = 1$), and we have two geometrical parameters, namely, l/h and d/h. We define $K_1 = \omega^* h^*/c_0^*$, to distinguish it from $K = \omega^* l^*/c_0^*$ used in the preceding section. In the following examples, the x axis is taken along the channel centerline. Under the no-flow assumption, symmetry and antisymmetry conditions may be applied about the x and y axes such that only the quarter-plane problem $x \geq 0$, $y \leq 0$ needs to be solved. The antisymmetric problem about the channel centerline, that is, $\phi(x, -y) = -\phi(x, +y)$, is termed the Dirichlet problem, because Dirichlet boundary conditions are imposed along the x axis. Consequently the symmetric problem $\phi(x, -y) = \phi(x, +y)$ is termed the Neumann problem. Linton and Evans[31] identified trapped or bound modes (i.e., modes with no radiation losses) for a duct with an indented wall below the first cutoff frequency. In all these confined cases a single PML in the x direction is sufficient to damp outgoing waves as shown in Fig. 1b.

A. Dirichlet Problem

Figure 6a shows the symmetric and antisymmetric Dirichlet resonances of a deep cavity with $l/d = 0.5$ confined in a channel with $d/h = 1$, $N_{x,\text{col}} = N_{y,\text{col}} = 35$, $d_x = 1.0$, $\sigma_{0,x} = 5.0$, $\beta = 1$, and $x_0 = 1.25$. Circles denote modes symmetric about the y axis, and triangles denote antisymmetric modes. At the cut-on frequencies $\text{Re}(K_1/2\pi) = (2n-1)/(2h)$ $(n = 1, 2, \ldots)$ of the Dirichlet modes, the discrete approximations of the continuous spectra start. The shaded area below the first cut-on frequency $\text{Re}(K_1/2\pi) = \frac{1}{2}$ marks

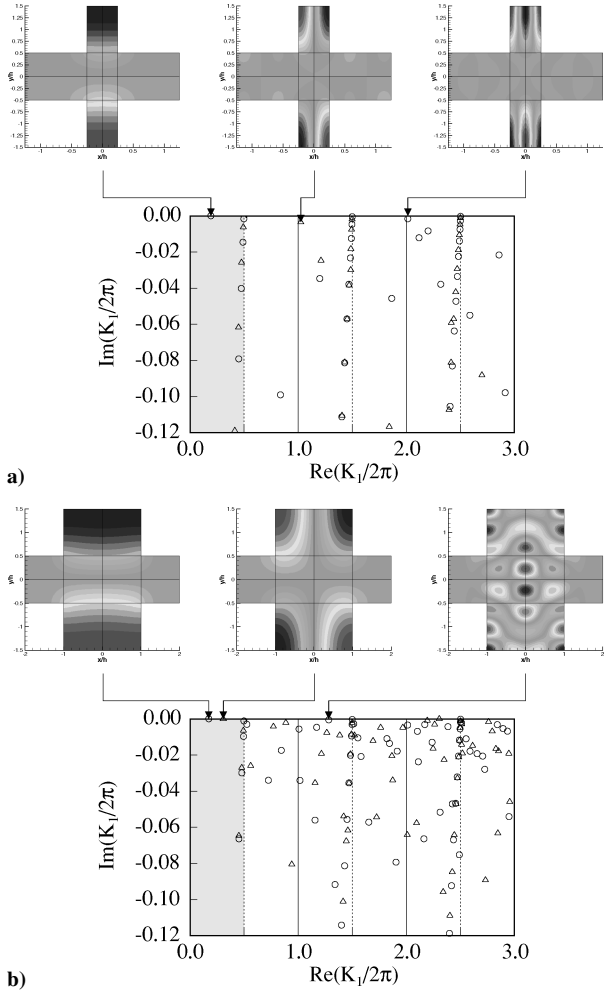

Fig. 6 Dirichlet confined ($d/h = 1$) cavity resonances with sample eigenfunctions: a) deep cavity, $l/d = 0.5$; and b) shallow cavity, $l/d = 2.0$.

the frequency domain where trapped modes are possible,[31] because in the wider channel $h + 2d$, formed by the cavities on both sides of the channel, the first antisymmetric duct mode is cut on, whereas it is cut off in the duct with $h = 1$. For $l/d = 0.5$ only the fundamental cavity mode is trapped. In addition to the eigenfunction of this (trapped) fundamental mode two more weakly damped modes are depicted, which correspond to the first antisymmetric and first symmetric cavity mode in Fig. 2a.

Corresponding to Fig. 2c we also depict the Dirichlet spectrum for a confined shallow cavity with $l/d = 2$ and $d/h = 1$ in Fig. 6b; $N_{x,\text{col}} = N_{y,\text{col}} = 35$, $d_x = 1.0$, $\sigma_{0,x} = 5.0$, $\beta = 1$, and $x_0 = 2.0$. Now two modes are trapped, namely, the fundamental and the first antisymmetric mode. In addition to the eigenfunction of these two undamped modes, we show the eigenfunction of another weakly damped mode that clearly is a cavity mode. However, there are also modes that extend into the duct and therefore are expected to be influenced by mean flow.

The results of iterative continuation of individual modes for $d/h = 1$ up to $l/h = 6$ with the lower resolution $N_{x,\text{col}} = N_{y,\text{col}} = 20$ are depicted in Fig. 7a. The solid lines depict the resonances of symmetric eigenfunctions, the dashed lines the resonances of antisymmetric eigenfunctions. The shaded area marks the region of genuinely trapped modes below the first cutoff. The open symbols mark the resonant frequencies of Figs. 6a and 6b with the higher resolution, providing a check of accuracy. With increasing l/h, more and more trapped modes are possible. Near $l/h \approx 1$ and $\text{Re}(K_1/2\pi) = \frac{5}{6}$ we observe an interesting modal exchange: the first symmetric longitudinal cavity mode changes into a (highly damped) depth mode as l/h decreases. The trapped-mode frequencies correspond to those plotted by Evans and Linton[31] in their Fig. 8. The only difference is that for $l/h \to 0$ the resonances are expected[25] to

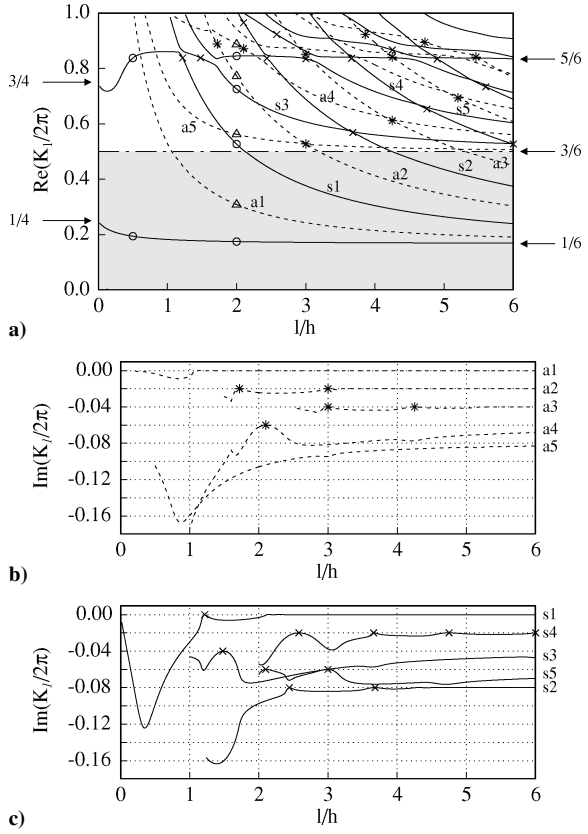

Fig. 7 Dirichlet confined ($d/h = 1$) cavity resonances: a) variation of resonant frequency $\mathrm{Re}(K_1/2\pi)$ with l/h; damping $\mathrm{Im}(K_1/2\pi)$ of b) antisymmetric and c) symmetric modes.

approach the one-dimensional organ pipe resonances $(2n-1)/(4d)$ $(n = 1, 2, \ldots)$ in the cavity, as marked on the left-hand side of Fig. 7a.

On the right-hand side of Fig. 7a the cut-on frequencies $(2n-1)/[2(h+2d)]$ $(n = 1, 2, \ldots)$ of the first three Dirichlet modes in the wider channel formed by cavities on both sides of the duct are marked. The damping $\mathrm{Im}(K_1/2\pi)$ of some antisymmetric and symmetric modes, as denoted on the right-hand side of the figures, is shown in Figs. 7b and 7c, respectively. All modes have zero damping as long as they are in the shaded region. For clearer distinction the y axis of each curve in Figs. 7b and 7c is shifted by -0.02. Nearly trapped modes, marked by crosses for symmetric modes and asterisks for antisymmetric modes, with vanishingly small radiation losses, occur near the cut-on frequency $\mathrm{Re}(K_1/2\pi) = \frac{5}{6}$ as well as between $\mathrm{Re}(K_1/2\pi) = \frac{3}{6}$ and $\mathrm{Re}(K_1/2\pi) = \frac{5}{6}$. Some of these might even be truely trapped modes with zero radiation: just before returning the revised version of this paper, Maureen McIver sent me a copy of the Ph.D. dissertation of Yuting Duan[43] (part of the results were presented in Ref. 44). By using a completely different method, Duan[43] showed that, besides the trapped Dirichlet modes of Evans and Linton[31] (with frequencies below the first cutoff frequency), embedded trapped modes (with frequencies above the first cutoff frequency) exist for both Dirichlet and Neumann resonances for particular parameter combinations. Unfortunately, the parameter ranges of the results computed by Duan and the ones shown here do not overlap so that no quick comparison is possible. However, for a related waveguide problem published by Linton and Ratcliffe[45] (Dirichlet modes) and Linton et al.[46] (Neumann modes), a comparison showed excellent agreement between their explicitly computed embedded trapped modes and our Parker mode resonances[35] with vanishingly small damping. (A similar comparison for the Parker mode problem can be found in Ref. 43.) Our numerical analysis cannot distinguish exactly between trapped modes and nearly trapped modes, but we expect that any resonance in Fig. 7a with very small damping can be excited easily by Rossiter modes, similar to the Parker modes[35,47] which are excited easily by vortices shed from objects in a duct.

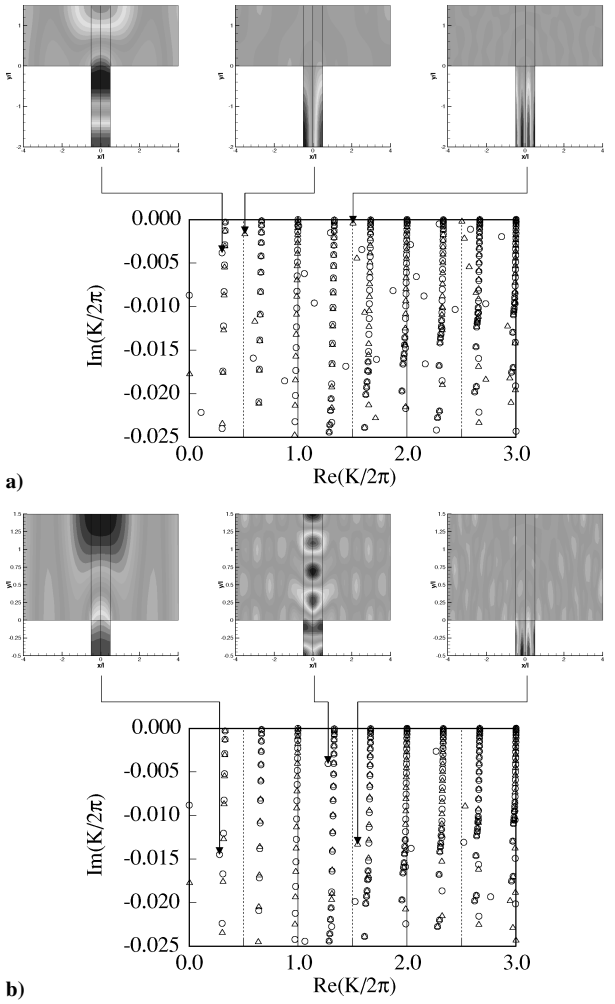

Fig. 8 Neumann confined ($h/l = 3$) cavity resonances with sample eigenfunctions: a) deep cavity, $l/d = 0.5$; and b) shallow cavity, $l/d = 2.0$.

B. Neumann Problem

In a cross junction the even Neumann modes are generally highly damped contrary to the odd Dirichlet modes[40] treated in the preceding section. However, if the cavity is located only on one side of the duct, as is usually the case for cavity wind-tunnel tests[6,22] or in dump combustors,[48] Neumann modes are the only ones present. To have a better comparison with the unconfined cavity results of Fig. 2 it is of advantage to choose $l^*_{\mathrm{ref}} = l^*$ as the reference length. Figure 8 shows the symmetric (circles) and antisymmetric (triangles) Neumann resonances for deep and shallow confined cavities with fixed $h/l = 3$, computed with $N_{x,\mathrm{col}} = N_{y,\mathrm{col}} = 35$, $d_x = 5.0$, $\sigma_{0,x} = 5.0$, $\beta = 1$, and $x_0 = 4.0$. The particular value $h/l = 3$ corresponds to the low-speed shallow-cavity experiment of Cattafesta et al.[22] Comparing the spectra of Fig. 8 with those of Fig. 2, we observe significant differences: the discrete approximations of the continuous spectra appear at the cut-on frequencies $\mathrm{Re}(K/2\pi) = n/(h/l)$ $(n = 1, 2, \ldots)$ of the Neumann modes. The continuous spectra in Fig. 8, which theoretically should be continuous lines, clearly show that the accuracy of our global eigenvalue computation deteriorates for resonances with larger real or imaginary parts. The spectral pattern is strikingly different from that of Fig. 2, because in addition to the cavity modes of Fig. 2 duct modes become important.

In Fig. 9 we compare the symmetric Neumann resonances for the confined cavity $h/l = 3$ with the unconfined cavity resonances of Fig. 3 (redrawn as solid curves) up to $\mathrm{Re}(K/2\pi) = 1$. The shaded regions mark the frequency domains with the same number of cut-on Neumann modes in the duct. The symmetric Neumann resonances of Fig. 8a for $l/d = 0.5$ are reshown in Fig. 9a by circles. We see that the $(0, 0)$ confined-mode resonance shifts to slightly higher frequencies. But more important, for large l/d, all confined modes approach the Neumann cut-on frequencies marked on the right-hand

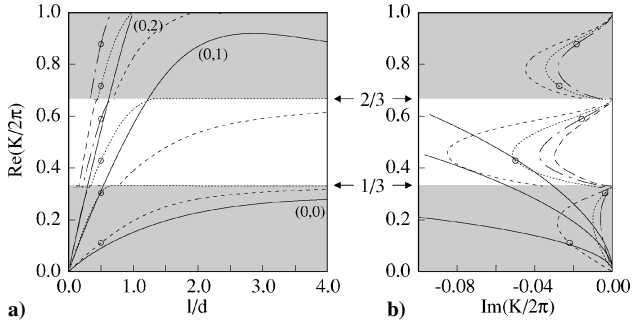

Fig. 9 Comparison between resonant frequencies of unconfined and Neumann confined ($h/l = 3$) cavities: a) variation of resonant frequency with l/d and b) damping Im($K/2\pi$) of resonant modes.

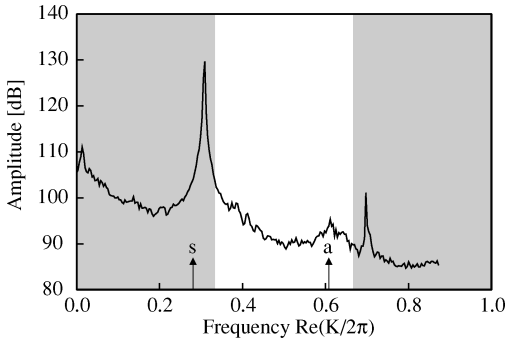

Fig. 10 Comparison of the measured amplitudes of Cattafesta et al.[22] at the first symmetric (s) and antisymmetric (a) resonance and the cut-on frequencies.

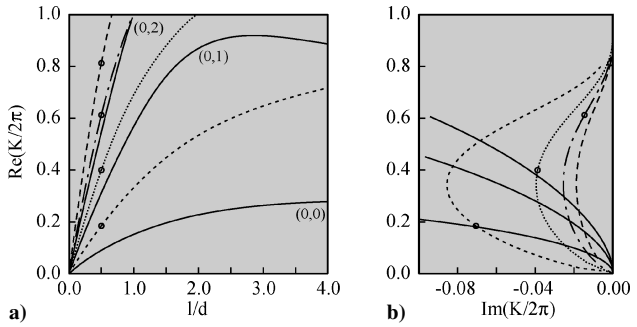

Fig. 11 Comparison between resonant frequencies of unconfined and Neumann confined ($h/l = 1$) cavities: a) variation of resonant frequency with l/d and b) damping Im($K/2\pi$) of resonant modes.

side of Fig. 9a. For example, with increasing l/d, the (0, 1) mode frequency at first follows the unconfined-cavity frequency very closely up to the first Neumann cut-on frequency $\mathrm{Re}(K/2\pi) = \frac{1}{3}$ and then merges with it. This duct mode is very weakly damped and the corresponding frequency agrees fairly well with the dominant frequency $f = 175$ Hz measured by Cattafesta et al.[22] for $l/d = 2$ and $h/l = 3$ in their low-speed test (cf. Fig. 10). Such a correlation between dominating mode frequency and duct cut-on frequency was documented already by Cattafesta et al.[49] in their Fig. 4.1.1.2 summarizing high-speed wind-tunnel results. This correlation with duct cut-on frequencies is a cause for concern because it means that the results for cavities confined in a hard-walled wind tunnel cannot be applied directly to unconfined cavities. Cattafesta et al.[49] mitigated this problem in their test by replacing the solid tunnel ceiling by an acoustic liner. Here we used only their results without duct lining.

In Fig. 9b we compare the damping Im($K/2\pi$) of the confined and unconfined resonances of the modes in Fig. 9a. The symbols in Figs. 9a and 9b should allow identification of corresponding modes. The solid curves again depict the unconfined resonances of Fig. 3b. Considerable differences are apparent between the damping of resonant modes in confined and unconfined cavities. Figures 11 and 12 show similar comparisons for $h/l = 1$ and 5, respectively. For all confined-cavity cases the least-damped resonances are close to

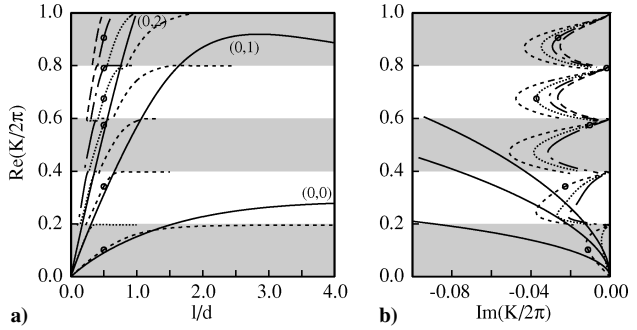

Fig. 12 Comparison between resonant frequencies of unconfined and Neumann confined ($h/l = 5$) cavities: a) variation of resonant frequency with l/d and b) damping Im($K/2\pi$) of resonant modes.

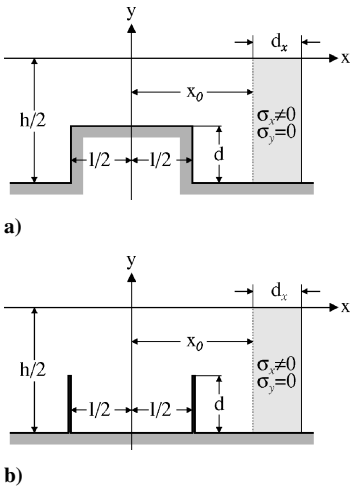

Fig. 13 Additional confined configurations: a) wall protrusion and b) pair of flow restrictors.

the duct cut-on frequencies. Near these cut-on frequencies we encountered numerical difficulties that are related to the passing of a discrete resonance through the continuous spectrum of the cut-on mode. Our numerical procedure cannot distinguish between a discrete resonance and the discrete approximation of the continuous spectrum. A more detailed study of the exact structure of this modal interaction should be of considerable interest.

We also used the method for the computation of resonances in other confined configurations, such as a single rectangular wall protrusion or a pair of flow restrictors in a duct as depicted in Fig. 13. In both examples resonances can be excited aerodynamically by shedding vortices and diagrams similar to Fig. 7 can be computed. For the orifice flow problem of Fig. 13a, a whistling phenomenon can occur if the thickness of the protrusion l is comparable with the hole diameter $h - 2d$ (Refs. 50 and 51) providing the source for exciting resonances. The example of flow restrictors (cf. Fig. 13b) is of considerable interest for segmented solid-propellant boosters[52–54] where these so-called inhibitors can cause high-amplitude oscillations. Results of these computations will be shown elsewhere.

V. Conclusions

We applied PML absorbing boundary conditions in the complex scaling form of atomic physics to numerically compute acoustic resonances in two-dimensional rectangular open cavities. For properly chosen PML parameters, this method worked very well and can be extended to three dimensions or open cavities with more general boundaries. Numerical difficulties were encountered only when a resonance interacted with a continuous spectrum, a situation that needs a more detailed investigation. We observed significant differences between resonances in confined and unconfined cavities with important implications for wind-tunnel testing of cavities. In a wind tunnel the duct cut-on frequencies as well as embedded trapped modes seem to dominate cavity resonances, which are quite different from the resonances of unconfined cavities.

Acknowlegments

This work was supported by the German Aerospace Research Program and the Volkswagenstiftung. The author is grateful to Lou Cattafesta for providing his detailed experimental data, to Chris Linton and Maureen McIver for making available their data for the trapped modes, and to Thorsten Hohage and Stefan Hein for helpful discussions. The critical comments of the three reviewers are gratefully acknowledged.

References

[1]Rockwell, D., and Naudascher, E., "Review—Self-Sustaining Oscillations of Flow Past Cavities," *Journal of Fluids Engineering*, Vol. 100, June 1978, pp. 152–165.

[2]Rockwell, D., and Naudascher, E., "Self-Sustained Oscillations of Impinging Free Shear Layers," *Annual Review of Fluid Mechanics*, Vol. 11, 1979, pp. 67–94.

[3]Rockwell, D., "Oscillations of Impinging Shear Layers," *AIAA Journal*, Vol. 21, No. 5, 1983, pp. 645–664.

[4]Blake, W., *Mechanics of Flow-Induced Sound and Vibration*, Vols. 1 and 2, Academic Press, New York, 1986.

[5]Plumblee, H., Gibson, J., and Lassiter, L., "A Theoretical and Experimental Investigation of the Aeroacoustic Response of Cavities in Aerodynamic Flow," WADD-TR-61-75, Wright–Patterson AFB, Dayton, OH, March 1962.

[6]Rossiter, J., "Wind-Tunnel Experiments on the Flow over Rectangular Cavities at Subsonic and Transonic Speeds," Aeronautical Research Council, Repts. and Memoranda 3438, London, Oct. 1966.

[7]Bilanin, A., and Covert, E., "Estimation of Possible Excitation Frequencies for Shallow Rectangular Cavities," *AIAA Journal*, Vol. 11, No. 3, 1973, pp. 347–351.

[8]Heller, H., and Bliss, D., "The Physical Mechanism of Flow-Induced Pressure Fluctuations in Cavities and Concepts for Their Suppression," AIAA Paper 75-491, March 1975.

[9]Tam, C., and Block, P., "On the Tones and Pressure Oscillations Induced by Flow over Rectangular Cavities," *Journal of Fluid Mechanics*, Vol. 89, 1978, pp. 373–399.

[10]Howe, M., "Edge, Cavity and Aperture Tones at Very Low Mach Numbers," *Journal of Fluid Mechanics*, Vol. 330, 1997, pp. 61–84.

[11]Alvarez, J., Kerschen, E., and Tumin, A., "A Theoretical Model for Cavity Acoustic Resonances in Subsonic Flow," AIAA Paper 2004-2845, May 2004.

[12]Ahuja, K., and Mendoza, J., "Effects of Cavity Dimensions, Boundary Layer, and Temperature on Cavity Noise with Emphasis on Benchmark Data to Validate Computational Aeroacoustic Codes," NASA CR 4653, April 1995.

[13]Alvarez, J., and Kerschen, E., "Influence of Wind Tunnel Walls on Cavity Acoustic Resonances," AIAA Paper 2005-2804, May 2005.

[14]Koch, W., "Acoustic Resonances in Rectangular Open Cavities," AIAA Paper 2004-2843, May 2004.

[15]Hein, S., Koch, W., and Schöberl, J., "Acoustic Resonances in a 2D High Lift Configuration and a 3D Open Cavity," AIAA Paper 2005-2867, May 2005.

[16]Hu, F., "On Using Perfectly Matched Layer for the Euler Equations with a Non-Uniform Mean Flow," AIAA Paper 2004-2966, May 2004.

[17]Hardin, J., and Pope, D., "Sound Generation by Flow over a Two-Dimensional Cavity," *AIAA Journal*, Vol. 33, No. 3, 1995, pp. 407–412.

[18]Rowley, C., Colonius, T., and Basu, A., "On Self-Sustained Oscillations in Two-Dimensional Compressible Flow over Rectangular Cavities," *Journal of Fluid Mechanics*, Vol. 455, 2002, pp. 315–346.

[19]Gharib, M., and Roshko, A., "The Effect of Flow Oscillations on Cavity Drag," *Journal of Fluid Mechanics*, Vol. 177, 1987, pp. 501–530.

[20]Krishnamurty, K., "Acoustic Radiation from Two-Dimensional Rectangular Cutouts in Aerodynamic Surfaces," NACA TN3487, Aug. 1955.

[21]Crighton, D., "Airframe Noise," *Aeroacoustics of Flight Vehicles: Theory and Practice. Vol. 1: Noise Sources*, edited by H. H. Hubbard, NASA, 1991, pp. 391–447.

[22]Cattafesta, L., III, Garg, S., Choudhari, M., and Li, F., "Active Control of Flow-Induced Cavity Resonance," AIAA Paper 97-1804, June 1997.

[23]Williams, D., Fabris, D., and Morrow, J., "Experiments on Controlling Multiple Acoustic Modes in Cavities," AIAA Paper 2000-1903, June 2000.

[24]Sarohia, V., "Experimental Investigation of Oscillations in Flows over Shallow Cavities," *AIAA Journal*, Vol. 15, No. 7, 1977, pp. 984–991.

[25]East, L., "Aerodynamically Induced Resonance in Rectangular Cavities," *Journal of Sound and Vibration*, Vol. 3, No. 3, 1966, pp. 277–287.

[26]Block, P., "Noise Response of Cavities of Varying Dimensions at Subsonic Speeds," NASA TN D-8351, Dec. 1976.

[27]Shaw, L., Bartel, H., and McAvoy, J., "Acoustic Environment in Large Enclosures with a Small Opening Exposed to Flow," *Journal of Aircraft*, Vol. 20, No. 3, 1983, pp. 250–256.

[28]Tam, C., "The Acoustic Modes of a Two-Dimensional Rectangular Cavity," *Journal of Sound and Vibration*, Vol. 49, No. 3, 1976, pp. 353–364.

[29]Raman, G., Envia, E., and Bencic, T., "Jet–Cavity Interaction Tones," *AIAA Journal*, Vol. 40, No. 8, 2002, pp. 1503–1511.

[30]Ziada, S., Ng, H., and Blake, C., "Flow Excited Resonance of a Confined Shallow Cavity in Low Mach Number Flow and Its Control," *Journal of Fluids and Structures*, Vol. 18, No. 1, 2003, pp. 79–92.

[31]Evans, D., and Linton, C., "Trapped Modes in Open Channels," *Journal of Fluid Mechanics*, Vol. 225, 1991, pp. 153–175.

[32]Bérenger, J., "A perfectly Matched Layer for the Absorption of Electromagnetic Waves," *Journal of Computational Physics*, Vol. 114, No. 2, 1994, pp. 185–200.

[33]Moiseyev, N., "Quantum Theory of Resonances: Calculating Energies, Widths and Cross-Sections by Complex Scaling," *Physics Reports*, Vol. 302, No. 5–6, 1998, pp. 211–293.

[34]Helmholtz, H., *On the Sensations of Tone*, 2nd ed., Dover, New York, 1954.

[35]Hein, S., Hohage, T., and Koch, W., "On Resonances in Open Systems," *Journal of Fluid Mechanics*, Vol. 506, 2004, pp. 255–284.

[36]Canuto, C., Hussaini, M., Quarteroni, A., and Zang, T., *Spectral Methods in Fluid Dynamics*, Springer-Verlag, New York, 1988.

[37]Zurmühl, R., *Matrizen und ihre technischen Anwendungen*, 3rd ed., Springer, Berlin, 1961.

[38]Kriesels, P., Peters, M., Hirschberg, A., Wijnands, A., Iafrati, A., Riccardi, G., Piva, R., and Bruggeman, J., "High Amplitude Vortex-Induced Pulsations in a Gas Transport System," *Journal of Sound and Vibration*, Vol. 184, No. 2, 1995, pp. 343–368.

[39]Ziada, S., and Shine, S., "Strouhal Numbers of Flow-Excited Acoustic Resonance of Closed Side Branches," *Journal of Fluids and Structures*, Vol. 13, No. 1, 1999, pp. 127–142.

[40]Dequand, S., Hulshoff, S., and Hirschberg, A., "Self-Sustained Oscillations in a Closed Side Branch System," *Journal of Sound and Vibration*, Vol. 265, No. 2, 2003, pp. 359–386.

[41]Keller, J., and Escudier, M., "Flow-Excited Resonances in Covered Cavities," *Journal of Sound and Vibration*, Vol. 86, No. 2, 1983, pp. 199–226.

[42]Lafon, P., Caillaud, S., Devos, J., and Lambert, C., "Aeroacoustical Coupling in a Ducted Shallow Cavity and Fluid/Structure Effects on a Steam Line," *Journal of Fluids and Structures*, Vol. 18, No. 6, 2003, pp. 695–713.

[43]Duan, Y., "Trapped Modes and Acoustic Resonances," Ph.D. Dissertation, Loughborough Univ., Jan. 2004.

[44]Duan, Y., and McIver, M., "Embedded Trapped Modes near an Indentation in an Open Channel," *17th International Workshop on Water Waves and Floating Bodies*, edited by R. S. F. Lee, Peterhouse, Cambridge, England, U.K., 2002, pp. 37–40.

[45]Linton, C., and Ratcliffe, K., "Bound States in Coupled Guides. I. Two Dimensions," *Journal of Mathematical Physics*, Vol. 45, No. 4, 2004, pp. 1359–1379.

[46]Linton, C., McIver, M., McIver, P., Ratcliffe, K., and Zhang, J., "Trapped Modes for Off-Centre Structures in Guides," *Wave Motion*, Vol. 36, No. 1, 2002, pp. 67–85.

[47]Parker, R., "Resonance Effects in Wake Shedding from Parallel Plates: Some Experimental Observations," *Journal of Sound and Vibration*, Vol. 4, No. 1, 1966, pp. 62–72.

[48]Najm, H., and Ghoniem, A., "Numerical Simulation of the Convective Instability in a Dump Combustor," *AIAA Journal*, Vol. 29, No. 6, 1991, pp. 911–919.

[49]Cattafesta, L., III, Garg, S., Shuklak, D., and Choudhari, M., "Prediction and Active Control of Flow-Induced Weapons Bay Acoustics," Final Technical Rept. to U.S. Air Force Research Lab., Air Vehicles Directorate, High Technology Corp., Hampton, VA, May 1999.

[50]Morse, P., and Ingard, K., *Theoretical Acoustics*, McGraw–Hill, New York, 1968, Fig. 11.21.

[51]Joksch, A., and Gravett, C., "Effect of the Vortex Whistle on the Discharge Coefficient of Orifices," *AIAA Journal*, Vol. 42, No. 5, 2004, pp. 1048–1050.

[52]Brown, R., Dunlap, R., Young, S., and Waugh, B., "Vortex Shedding as a Source of Acoustic Energy in Segmented Solid Rockets," *Journal of Spacecraft and Rockets*, Vol. 18, No. 4, 1981, pp. 312–319.

[53]Stubos, A., Benocci, C., Palli, E., Stoubos, G., and Olivari, D., "Aerodynamically Generated Acoustic Resonance in a Pipe with Annular Flow Restrictors," *Journal of Fluids and Structures*, Vol. 13, No. 6, 1999, pp. 755–778.

[54]Anthoine, J., Mettenleiter, M., Repellin, O., Buchlin, J.-M., and Candel, S., "Influence of Adaptive Control on Vortex-Driven Instabilities in a Scaled Model of Solid Propellant Motors," *Journal of Sound and Vibration*, Vol. 262, No. 5, 2003, pp. 1009–1046.

D. Gaitonde
Associate Editor